Article

The Innovative Polygon Trend Analysis (IPTA) as a Simple Qualitative Method to Detect Changes in Environment—Example Detecting Trends of the Total Monthly Precipitation in Semiarid Area

Mohammed Achite [1,2], Gokmen Ceribasi [3], **Ahmet Iyad Ceyhunlu [3]**, **Andrzej Wałęga [4,*]** **and Tommaso Caloiero [5]**

[1] Laboratory of Water & Environment, Faculty of Nature and Life Sciences, University Hassiba Benbouali of Chlef, Ouled Fares, Chlef 02180, Algeria; m.achite@univ-chlef.dz
[2] National Higher School of Agronomy, ENSA, Hassan Badi, El Harrach, Algiers 16200, Algeria
[3] Department of Civil Engineering, Faculty of Technology, Sakarya University of Applied Sciences, Sakarya 54050, Turkey; gceribasi@subu.edu.tr (G.C.); ahmetceyhunlu@subu.edu.tr (A.I.C.)
[4] Department of Sanitary Engineering and Water Management, University of Agriculture in Krakow, Mickiewicza 24/28 Street, 30-059 Krakow, Poland
[5] National Research Council of Italy, Institute for Agriculture and Forest Systems in the Mediterranean (CNR-ISAFOM), Via Cavour 4/6, 87036 Rende, CS, Italy; tommaso.caloiero@isafom.cnr.it
* Correspondence: andrzej.walega@urk.edu.pl; Tel.: +48-012-662-4102

Abstract: Precipitation is a crucial component of the water cycle, and its unpredictability may dramatically influence agriculture, ecosystems, and water resource management. On the other hand, climate variability has caused water scarcity in many countries in recent years. Therefore, it is extremely important to analyze future changes of precipitation data in countries facing climate change. In this study, the Innovative Polygon Trend Analysis (IPTA) method was applied for precipitation trend detection at seven stations located in the Wadi Sly basin, in Algeria, during a 50-year period (1968–2018). In particular, the IPTA method was applied separately for both arithmetic mean and standard deviation. Additionally, results from the IPTA method were compared to the results of trend analysis based on the Mann–Kendall test and the Sen's slope estimator. For the different stations, the first results showed that there is no regular polygon in the IPTA graphics, thus indicating that precipitation data varies by years. As an example, IPTA result plots of both the arithmetic mean and standard deviation data for the Saadia station consist of many polygons. This result means that the monthly total precipitation data is not constant and the data is unstable. In any case, the application of the IPTA method showed different trend behaviors, with a precipitation increase in some stations and decrease in others. This increasing and decreasing variability emerges from climate change. IPTA results point to a greater focus on flood risk management in severe seasons and drought risk management in transitional seasons across the Wadi Sly basin. When comparing the results of trend analysis from the IPTA method and the rest of the analyzed tests, good agreement was shown between all methods. This shows that the IPTA method can be used for preliminary analysis trends of monthly precipitation.

Keywords: precipitation; innovative polygon trend analysis; arithmetic mean; standard deviation; Wadi Sly; Algeria

1. Introduction

Precipitation can be considered among the major variables that are frequently used to trace the extent and magnitude of climate variability [1]. In fact, Gautam et al. [2] and Chen et al. [3] showed that hanging patterns of precipitation are among the chief consequences attributed to climate variability.

In particular, precipitation seasonality and variability are important factors to understand in hydrological processes in a catchment; they are paramount for many sectors of the economy, like agricultural [4], and they have serious environmental implications that can greatly influence the food security and ecological sustainability of the different regions on the world [5]. The influence of precipitation on the environment can be altered by land cover, especially by forest. Juez et al. [6] showed that forest can influence hydrological dynamics and delay catchments response on high precipitation. Moreover, overland flow can occur rarely because of the strong infiltration rate [7]; a strong influence reduces evapotranspiration, and thus, increases low flow [8] as well as reduces nutrient and sediment load [9]. An increase of forest area in catchments can also protect against the effect of climate change on water resources.

Within this context, long-term data with different time resolutions are used to evaluate precipitation variability [10–13] that is linked with synoptic conditions and large-scale circulation [14,15], e.g., phase pace of NAO (North Atlantic Oscillation) teleconnection patterns [16,17] and sea surface temperature (SST) anomalies [18,19]. In particular, the Mediterranean region is affected by high precipitation variability, at both a temporal and spatial scale, due to its geographical position between two strongly contrasting masses of water: the Atlantic Ocean and the Mediterranean Sea [20]. An Additional feature determining high variability of precipitation in this region is the presence of various mountain ranges distributed along the coastal areas from east to west [21]. For example, in the Macta basin (Algeria), Elouissi et al. [22] observed decreasing trends of monthly precipitations in the northern part, close to the Mediterranean Sea coastal area, and increasing ones in the southern part. Based on the Coupled Model Intercomparison Project phase 6 (CMIP6), Bogcaci et al. [23] identified increasing precipitation projection in winter and spring over the east of the Black Sea Region and north-east of Anatolia, with a consequent increase in flood risk. El-Geizry [24] detected high seasonal variations of precipitation in the southern Levantine Basin, Egypt.

To detect temporal changes of hydroclimatological phenomena, trend analyses are the most common methods used. These analyses can help monitor global changes in different environmental components. Moreover, they are very important especially in semiarid regions where high risk of water scarcity occurrs; thus, the knowledge about the hydro-meteorology phenomena behavior can be used in water resources management and planning. Generally, trend analysis is based on non-parametric tests, such as the Mann–Kendall test or Sen's slope methods, which are more appropriate than parametric ones to deal with non-normally distributed data [25,26]. These tests have some limitations, linked with the null hypothesis (H_0) [27], which assumes serial correlation of data [28,29]. Serinaldi et al. [30] showed that even if the empirical estimation of trends based on commonly statistical tests is always feasible from a numerical point of view, it has poor information sources of non-stationarity without assuming a priori additional information on the underlying stochastic process.

With the aim to overcome such a problem, the Innovative Trend Analysis (ITA) was proposed [31] and applied in several studies on precipitation variability worldwide. For example, Caloiero et al. [32], Caloiero [33], Gedefaw et al. [34], Haktanir and Citakoglu [35], and Malik et al. [36] applied this methodology on monthly, seasonal, and annual precipitation series of India, Ethiopia, Italy, New Zealand, and Turkey, respectively. Due to the large use of the ITA, recently, some updates of this method have been proposed, such as the Innovative Triangular Trend Analysis (ITTA) and the Innovative Polygon Trend Analysis (IPTA) [37–39]. In particular, the IPTA [40] is an approach that helps to identify the trend in a given series and also trend transitions between successive sections of two equal segments from the original hydro-meteorological time series leading to trend polygon. Therefore, it constitutes a productive basis for finer interpretations with linguistic and numerical interpretations and inferences from a given time series.

The purpose of this study is to investigate trends of monthly total precipitation data of seven selected precipitation monitoring stations in the Wadi Sly basin in north Algeria

for the period 1968–2018. With this aim, the Innovative Polygon Trend Analysis (IPTA) technique was applied [40]. Moreover, results from the IPTA method were compared with results of trend analysis based on commonly known methods like the Mann–Kendall test (MK) and the Sen's estimator (SS).

2. Materials and Methods

2.1. Study Area

The Wadi Sly basin is located in the northwest of Algeria and has an area of 1225 km^2. It is a basin characterized by a typically semi-arid Mediterranean climate, with warm summers and cold winters. The database used in this study consists of seven high-quality and complete monthly precipitation series ranging from 1968–2018, with an average density of one station per 175 km^2 (Figure 1).
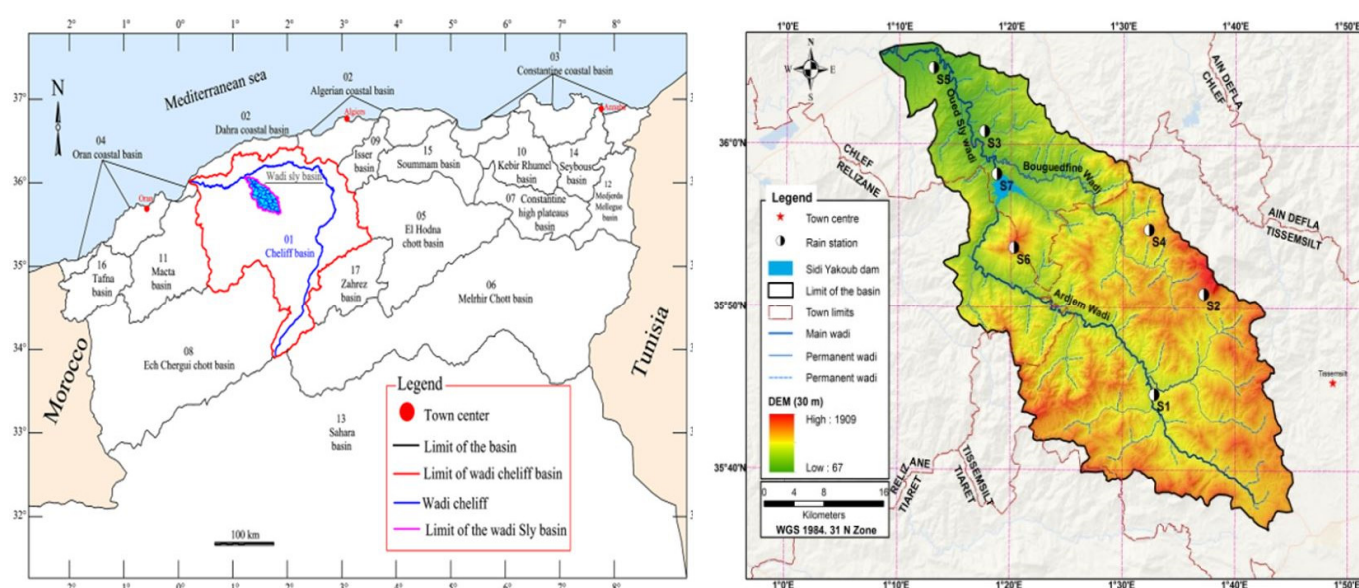

Figure 1. Localization of the selected rain gauges on DEM.

2.2. Data Analysis

The National Agency of Water Resources (ANRH) contributed data for this study from seven precipitation stations across Wadi Sly basin (Figure 1 and Table 1), each having long-term monthly precipitation records from 1968 to 2018.

Table 1. Precipitation Stations Characteristics.

Stations	ID	Name	Longitude (°)	Latitude (°)	Elevation (m)	Period of Observation
S1	012304	Souk El Had	1.55	35.75	550	1968/69–2017/18
S2	012306	Bordj Bounaama	1.62	35.85	1050	1968/69–2017/18
S3	012307	Ain Lellou	1.54	35.93	900	1968/69–2017/18
S4	012308	Ouled Ben A.E.K.	1.27	36.03	160	1968/69–2017/18
S5	012309	Oued Sly	1.20	36.09	95	1968/69–2017/18
S6	012316	SAADIA	1.34	35.90	1000	1968/69–2017/18
S7	012318	Sidi Yagoub Bge	1.32	35.97	202	1968/69–2017/18

However, the duration of these stations' records varies, and some have missing records; as a result, only observation stations with data series covering 70% or more of the whole period were chosen for our study in order to improve data quality. The data was subject to quality control and data gap filling using linear regression.

The descriptive statistics of monthly and annual precipitation in the Wadi Sly basin are shown in Table 2. According to these statistics, winter can be identified as the rainiest season for all the stations, with more than 40% of the total annual precipitation falling in this season.

Table 2. Descriptive statistics of monthly and annual precipitation (mm) in the Wadi Sly basin (1968–2018).

		Sep.	Oct.	Nov.	Dec.	Jan.	Feb.	Mar.	Apr.	May	Jun.	Jul.	Aug.	Year
S1	Min	0.00	0.00	0.00	0.00	0.00	0.00	0.00	0.00	0.00	0.00	0.00	0.00	153.00
	Max	78.60	221.70	184.70	258.00	253.60	175.90	209.30	102.40	71.10	33.00	28.50	31.30	819.50
	Mean	15.57	32.48	45.22	56.27	66.44	53.94	46.50	34.60	20.39	3.80	1.34	2.40	378.95
	SD	16.90	37.58	39.18	50.95	53.13	45.26	39.66	26.12	22.84	8.00	4.75	6.48	155.73
	C (%)	4.11	8.57	11.93	14.85	17.53	14.23	12.27	9.13	5.38	1.00	0.35	0.63	100.00
S2	Min	0.00	0.50	0.00	0.00	0.00	0.00	0.00	0.00	0.00	0.00	0.00	0.00	172.07
	Max	75.00	170.90	153.70	189.80	247.60	251.70	216.00	176.59	155.74	81.20	16.10	48.00	763.40
	Mean	16.80	38.82	55.34	60.97	65.67	60.50	59.98	56.37	25.80	7.68	0.83	2.43	451.21
	SD	17.54	42.33	40.77	41.72	52.91	59.25	47.01	53.45	37.86	17.14	2.59	7.88	148.17
	C (%)	3.72	8.60	12.26	13.51	14.55	13.41	13.29	12.49	5.72	1.70	0.18	0.54	100.00
S3	Min	0.00	0.00	0.00	0.00	0.59	4.00	6.10	0.00	0.00	0.00	0.00	0.00	212.31
	Max	62.40	150.58	193.60	138.70	191.30	133.90	158.60	154.00	197.30	58.60	17.40	31.80	687.49
	Mean	17.23	35.83	55.77	53.83	77.64	57.52	62.44	42.43	25.58	4.89	0.84	2.46	436.47
	SD	16.61	32.87	46.92	28.36	53.02	36.59	35.16	35.40	41.87	10.20	2.74	6.82	122.71
	C (%)	3.95	8.21	12.78	12.33	17.79	13.18	14.31	9.72	5.86	1.12	0.19	0.56	100.00
S4	Min	0.00	0.00	0.00	0.00	0.00	0.00	0.00	0.00	0.00	0.00	0.00	0.00	177.60
	Max	68.40	219.35	116.10	102.00	166.30	140.60	122.59	165.40	105.05	39.54	13.20	52.80	612.40
	Mean	15.37	31.10	44.96	43.73	45.89	48.16	47.60	39.91	25.52	6.37	1.00	3.24	352.87
	SD	16.02	40.67	28.17	26.93	32.17	36.43	32.68	36.71	25.82	9.48	2.57	10.11	100.74
	C (%)	4.35	8.81	12.74	12.39	13.00	13.65	13.49	11.31	7.23	1.81	0.28	0.92	100.00
S5	Min	0.00	0.00	0.00	1.48	0.00	0.00	0.00	0.00	0.00	0.00	0.00	0.00	129.60
	Max	37.90	123.00	94.70	112.00	151.30	118.00	110.40	125.90	146.80	24.55	16.55	23.00	466.01
	Mean	9.33	24.73	39.84	39.55	42.86	43.94	39.91	26.65	20.51	4.90	1.39	1.84	295.46
	SD	9.81	23.96	23.30	27.83	30.35	34.28	30.32	26.10	28.68	7.38	3.50	4.31	81.08
	C (%)	3.16	8.37	13.48	13.39	14.51	14.87	13.51	9.02	6.94	1.66	0.47	0.62	100.00
S6	Min	0.00	0.00	0.65	0.00	0.00	7.65	0.00	0.00	0.00	0.00	0.00	0.00	173.74
	Max	117.00	308.45	211.53	231.30	181.40	170.70	214.30	197.90	96.00	43.10	34.24	27.90	881.27
	Mean	23.33	44.60	66.47	75.18	68.44	72.81	69.59	42.07	21.64	7.03	2.56	2.29	496.03
	SD	26.54	54.42	55.58	51.13	51.83	46.77	48.95	49.04	27.95	11.46	6.38	5.87	157.77
	C (%)	0.05	0.09	0.13	0.15	0.14	0.15	0.14	0.08	0.04	0.01	0.01	0.00	1.00
S7	Min	0.00	0.10	0.00	0.00	1.80	0.00	0.00	0.00	0.00	0.00	0.00	0.00	136.05
	Max	68.70	165.20	127.60	105.50	167.70	95.38	107.40	134.80	75.30	31.70	14.70	19.10	543.13
	Mean	12.98	24.17	40.48	35.60	43.19	40.45	39.62	39.01	21.88	5.58	1.19	2.40	306.56
	SD	14.53	29.16	29.20	26.13	29.19	28.74	27.41	36.73	18.96	8.65	2.81	4.18	91.85
	C (%)	4.23	7.88	13.21	11.61	14.09	13.19	12.92	12.72	7.14	1.82	0.39	0.78	100.00

SD = Standard deviation; C (%) = Contribution, in percentage, to the total annual precipitation.

2.3. Innovative Polygon Trend Analysis Method

The IPTA was first proposed by Sen et al. [40]. For monthly precipitation records, given a series $x_1, \ldots, x_n$ of n years, the following monthly matrix was constructed:

$$
\begin{bmatrix}
x_{1,1}, & x_{1,2}, & . & & . & . & x_{1,12} \\
x_{2,1}, & x_{1,2}, & . & & . & . & x_{1,12} \\
. & . & . & & . & . & . \\
x_{i,1}, & x_{i,2}, & . & & . & . & x_{i,12} \\
. & . & . & & . & . & . \\
x_{n,1}, & x_{n,2}, & . & & . & . & x_{n,12}
\end{bmatrix}
\tag{1}
$$

Then, the matrix was divided in two halves, the upper part (the first) for $i = 1, \ldots, n/2$ and the lower part (the second) for $i = n/2 + 1, \ldots, n$, respectively, and the next 12 sets of parameters (e.g., arithmetic mean, standard deviation, skewness coefficient, maximum, minimum, etc.) providing detailed information about the monthly precipitation variations, were calculated for each subseries. Results of this analysis are represented in a Cartesian system in which the first series is placed on the X-axis and the second series is placed on the Y-axis (Figure 2).
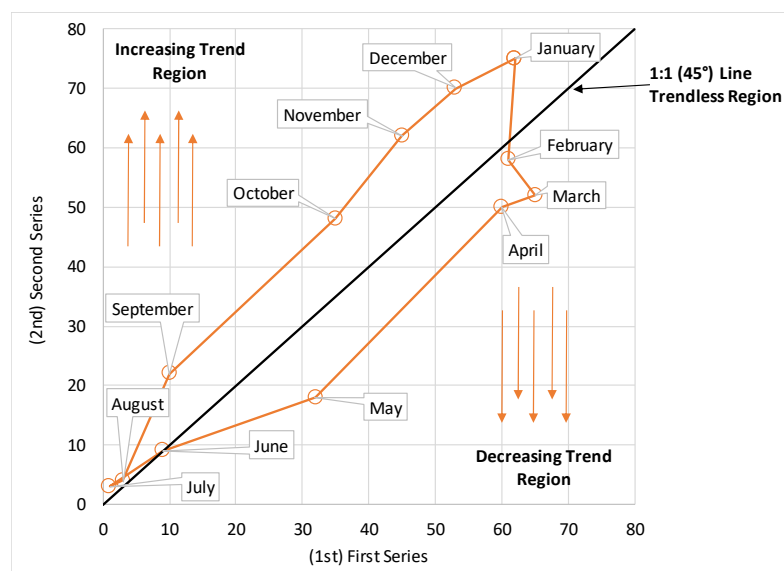

Figure 2. Hypothetical Innovative Polygon Trend Analysis template for monthly records.

As a consequence, the transition from 1 month's precipitation to the next is visible. Given the monthly precipitation distribution in the Cartesian system, homogeneity precipitation (single polygon) or non-homogeneity structure (multiple polygons) can be identified. Detailed information about the IPTA method can be found in Sen et al. [40].

2.4. The Mann-Kendal Test

The Mann–Kendall method is a non-parametric test for detecting trends in climatological and hydrological time series.

The Mann–Kendall test statistic S is calculated with the following equation [41,42]:

$$S = \sum_{k=1}^{n-1} \sum_{j=k+1}^{n} sgn\left(P_j - P_k\right) \tag{2}$$

where n is the number of data. P is the precipitation values at times i and j ($j > i$), and *sgn* is the sign function given as:

$$sgn\left(P_j - P_k\right) = \begin{cases} +1 \; if\left(P_j - P_k\right) > 0 \\ 0 \; if\left(P_j - P_k\right) = 0 \\ -1 \; if\left(P_j - P_k\right) < 0 \end{cases} \tag{3}$$

The variance of S is computed by

$$Var(S) = \frac{[n(n-1)(2n+5)] - \sum_{i=1}^{m} t_i(t_i - 1)(2t_i + 5)}{18} \tag{4}$$

where t_i is the number of ties of extent i, and m is the number of tied rank groups. For n larger than 10, the standard normal Z test statistic is computed as the Mann–Kendall test statistic as follows:

$$Z = \begin{cases} \frac{S-1}{\sqrt{Var(S)}} & if \ S > 0 \\ 0 \ if \ S = 0 \\ \frac{S-1}{\sqrt{Var(S)}} & if \ S < 0 \end{cases} \tag{5}$$

2.5. The Sen's Estimator

If a linear trend is observed in a time series, then the Sen's slope estimator can be used [43]. The slope estimates of N pairs of precipitation pairs are computed based on equation:

$$Qi = \frac{Pj - Pi}{j - i} \ for \ i = 1.2, \ldots, N \tag{6}$$

where P_j and P_i are the precipitation values at time j and i ($j > i$), respectively. The median of these N values of Q_i is the Sen's estimator of slope. The Sen's estimator is calculated by:

$$Q_{med} = \frac{1}{2}\left(Q_{\frac{N}{2}} + Q_{\frac{N+2}{2}}\right) \ if \ N \ is \ even \tag{7}$$

$$Q_{med} = \left(Q_{\frac{N+1}{2}}\right) \ if \ N \ is \ odd \tag{8}$$

3. Results and Discussion

3.1. IPTA Method

In this study, precipitation data from seven rain gauges in the Wadi Sly basin are analyzed using IPTA method. Figure 3 shows, for each station, the results of the IPTA method applied to the arithmetic mean data. Except for Bordj Bou Naama station, the IPTA charts of the other stations do not show a regular polygon. This is due to the fact that the arithmetic average of the monthly total precipitation data is not constant and the data does not change systematically. However, the fact that there is only one polygon at Bordj Bou Naama station, although not a regular one, indicates that the arithmetic mean of the monthly total precipitation data is generally stable. When the IPTA graph of this station is examined in detail on a monthly basis, it is seen that the months without a trend are October, December, June, July, and August. While an increasing trend is observed in September, November, and January, decreasing trends are observed in the remaining 4 months. This complex precipitation pattern can be explained considering the orographic factor and the geographic position of the basin in the Mediterranean, which is exposed to mid-latitude weather in winter and chronically challenged by subtropical dryness in summer. The seasonal trend behavior in precipitation at the Wadi Sly basin confirms the one detected by Achite and Caloiero [44] that evidenced a marked negative trend in spring and a less clear negative trend in winter. As described by Dettinger and Cayan [45] and by Polade et al. [46], precipitation in this region is characterized by typically infrequent frontal storms confined to the cold season. Precipitation changes over the Wadi Sly basin are similar to the ones in the Mediterranean region that can be explained by dynamical factors associated with changes in storm tracks and weather regimes, along with thermodynamic factors associated with increased water vapor content in a warmer atmosphere [47]. Meddi et al. [48] showed that in Algeria the temporal variability of the annual precipitation in the west of the country is influenced by ENSO, while Tramblay et al. [49] evidenced that precipitation in North Africa is mainly affected by the NAO.

General evaluation of arithmetic mean analysis results for each station in Figure 3 are given in Table 3.
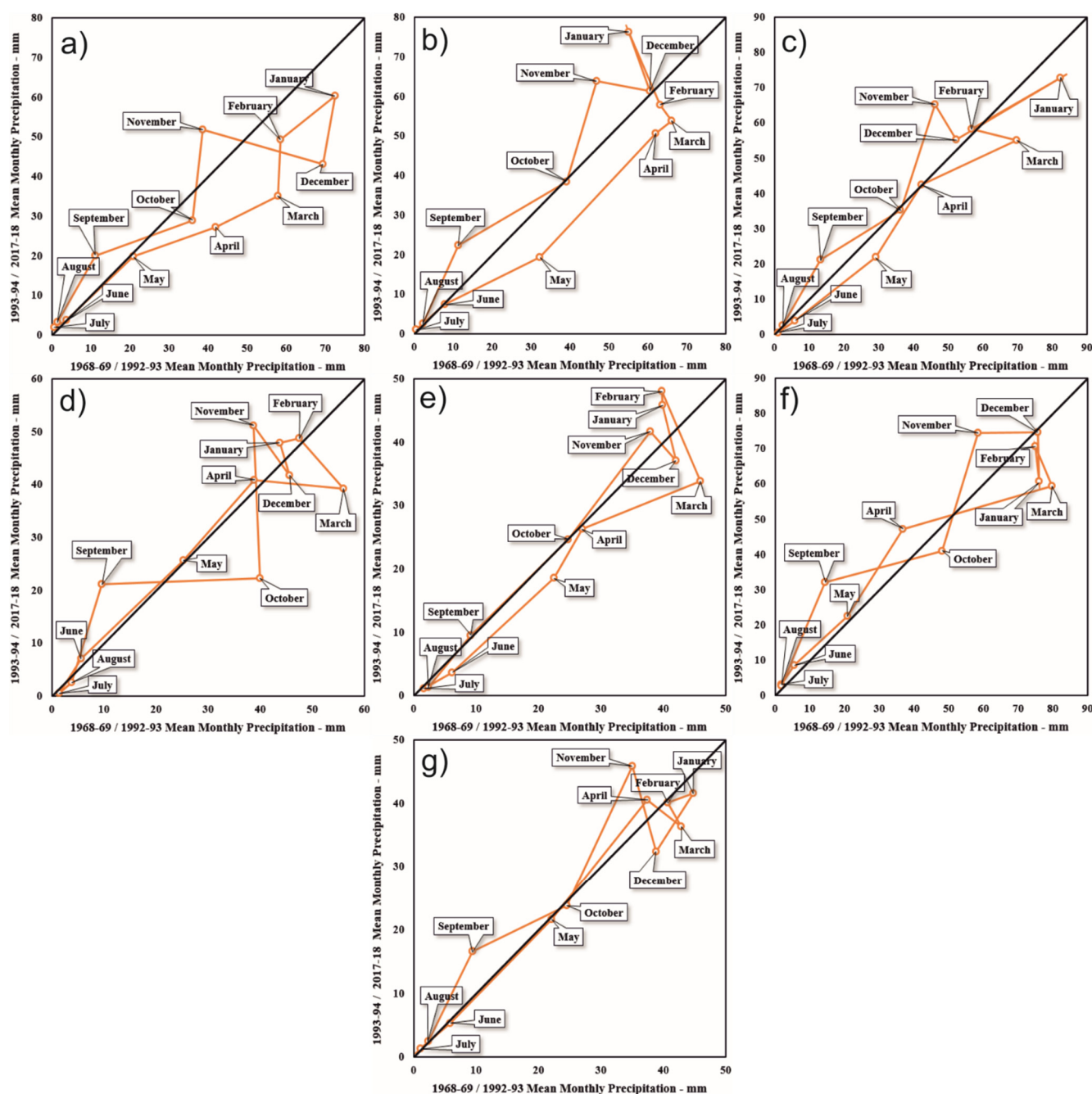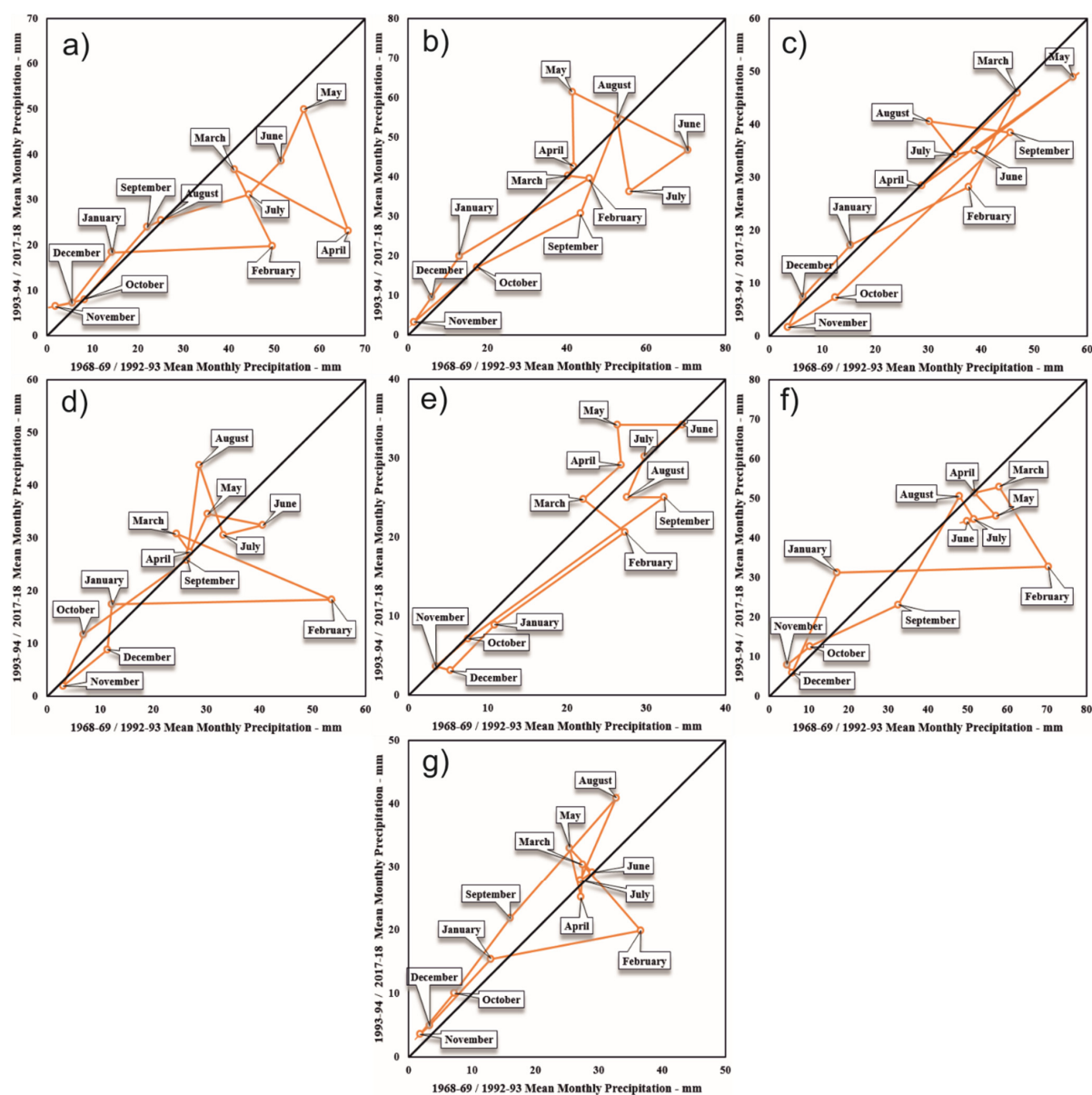
Figure 3. Innovative Polygon Trend Analysis Method graphics of arithmetic mean analysis results for each station: (**a**) Souk El Had, (**b**) Bordj Bou Naama, (**c**) Ain Lellou, (**d**) Ouled Ben A.E.K., (**e**) Oued Sly, (**f**) Saadia, and (**g**) Sidi Yakoub Bge.

Results generally evidenced four different behaviors of arithmetic mean of monthly precipitation in the Wady Sly basin: increasing precipitation trend in September and November; decreasing trend in March; mixed trend in October, December, January, February, April, May, and June; and no trend in July and August. The presented results are supported by Driouech et al. [50] who focused on observed evolutions and climate projections in Tunisia and Morocco. These Authors showed a trend towards drier conditions in the north-western part (Morocco) with a decrease in annual mean precipitation due to winter and spring negative trends similar to the ones detected in the Wady Sly basin (decreasing precipitation trend in winter and spring months). Figure 4 shows the results of the IPTA method applied to the standard deviation data of each station.

Table 3. General evaluation of arithmetic mean analysis results for each station.

Stations	Sep.	Oct.	Nov.	Dec.	Jan.	Feb.	Mar.	Apr.	May	Jun.	Jul.	Aug.
Souk El Had	↗	↘	↗	↘	↘	↘	↘	↘	→	→	→	→
Bordj Bou Naama	↗	→	↗	→	↗	↘	↘	↘	↘	→	→	→
Ain Lellou	↗	→	↗	↗	↘	→	↘	→	↘	↘	→	→
Ouled Ben A.E.K.	↗	↘	↗	↘	↗	↗	↘	↗	→	↗	→	→
Oued Sly	→	→	↗	↘	↗	↗	↘	→	↘	↘	→	→
Saadia	↗	↘	↗	→	↘	↘	↘	↗	→	↗	→	→
Sidi Yakoub Bge	↗	→	↗	↘	↘	→	↘	↗	→	→	→	→

↘ : Decreasing Trend.   ↗ : Increasing Trend.   → : No Trend.

Figure 4. Innovative Polygon Trend Analysis Method graphics of standard deviation analysis results for each station: (**a**) Souk El Had, (**b**) Bordj Bou Naama, (**c**) Ain Lellou, (**d**) Ouled Ben A.E.K., (**e**) Oued Sly, (**f**) Saadia, and (**g**) Sidi Yakoub Bge.

As in Figure 3, IPTA graphs of other stations except for Bordj Bou Naama station in Figure 4 do not show a regular polygon. This is due to the fact that the standard deviation of the monthly total precipitation data is not constant and the data does not change systematically. However, the fact that there is only one polygon at Bordj Bou Naama station, although not a regular one, indicates that the standard deviation of the monthly total precipitation data is generally stable. When the IPTA graph of this station is examined in detail on a monthly basis, it is seen that the months without a trend are October, March, and April. While an increasing trend is observed in November, December, January, May, and August, decreasing trends are observed in the remaining 4 months. In addition, in the autumn–winter period (October–January), the standard deviation trend of the mean monthly precipitation is less than in spring and summer months. In fact, during summer, precipitation is scarce but during summer, precipitation has high intensities, thus standard deviation of monthly precipitation is higher than in the rest of the year. In this season, the Azores anticyclone moves north but when the anticyclone retreats south, it lets in the ocean disturbances affecting North Africa [51].

A synthesis of the results showed in Figure 4 is given in Table 4.

Table 4. General evaluation of standard deviation analysis results for each station.

Stations	Sep.	Oct.	Nov.	Dec.	Jan.	Feb.	Mar.	Apr.	May	Jun.	Jul.	Aug.
Souk El Had	↗	↘	↗	↗	↗	↘	↘	↘	↘	↘	↘	→
Bordj Bou Naama	↘	→	↗	↗	↗	↘	→	→	↗	↘	↘	↗
Ain Lellou	↘	↘	↘	→	↗	↘	→	→	↘	↘	→	↗
Ouled Ben A.E.K.	→	↗	→	↘	↗	↘	↗	→	→	↘	↘	↗
Oued Sly	↘	→	→	↘	↘	↘	↗	↗	↗	→	→	↘
Saadia	↘	↗	↗	→	↘	↘	↘	→	↘	↘	↘	↗
Sidi Yakoub Bge	↗	↗	↗	↗	↗	↘	↗	↘	↗	→	→	↗

↘: Decreasing Trend.　↗: Increasing Trend.　→: No Trend.

Generally, increasing trends of standard deviations have been observed in January and August in five stations. An interesting behavior as observed in February with a decreasing trend of standard deviation monthly precipitations in all the stations. The more stable conditions were observed in April, where the majority of the stations did not evidence trends. As a result, the analysis of standard deviation trends of monthly precipitation evolution showed significant variability typical of the Mediterranean climate [52].

Statistical values of the arithmetic mean (AM) and the standard deviation (SD) for the seven stations are given in Tables 5 and 6, respectively. Results indicate transition between months. The maximum values are considered as an abrupt transition between 2 months.

Detailed results of the statistical values of the arithmetic mean (Table 5) for the Souk El Had station evidenced that the maximum trend length is 31.95 mm in the transition November–December, while a maximum trend slope of 21.17 was identified in February–March. For the Bordj Bou Naama station, the maximum trend length and slope are respectively 43.25 mm (April–May) and 3.32 (October–November). A maximum trend length of 34.78 mm and a maximum trend slope of 3.00 were detected in the Ain Lellou Mf station for the transitions December–January and October–November, respectively. As regards the Ouled Ben A.E.K. station, the maximum trend length was identified in September–October (30.35 mm), while the maximum trend slope was in October–November (−24.42). For the Oued Sly station, the maximum trend length is 22.10 mm (May–Jun.), and maximum trend slope is calculated as −40.54 (Jan.–Feb.). In the Saadia station, in March–April, a maximum trend length of 44.61 mm and a maximum trend slope of −25.76 in December–January were evaluated. Finally, in October–November, a maximum trend

length of 24.49 mm and maximum trend slope of 2.11 were identified in the Sidi Yakoub Bge station.

Table 5. Statistical values of arithmetic mean for each station.

		Sep.–Oct.	Oct.–Nov.	Nov.–Dec.	Dec.–Jan.	Jan.–Feb.	Feb.–Mar.	Mar.–Apr.	Apr.–May	May–Jun.	Jun.–Jul.	Jul.–Aug.	Aug.–Sep.
S1	Length (mm)	26.44	23.01	31.95	17.49	17.81	14.22	17.76	22.3	23.46	3.61	1.55	19.25
	Slope	0.36	8.76	−0.28	5.49	0.78	21.17	0.5	0.35	0.94	0.58	1.6	1.72
S2	Length (mm)	32.22	26.52	13.98	15.9	20.17	4.95	5.14	43.25	27.13	9.7	2.26	21.68
	Slope	0.58	3.32	−0.18	−2.71	−2.27	−1.36	0.77	1.05	0.48	0.87	0.91	2.18
S3	Length (mm)	27.05	31.55	11.7	34.78	29.52	13.49	30.21	24.39	29.48	5.83	2.34	21.59
	Slope	0.61	3	−1.64	0.59	0.57	−0.25	0.46	1.56	0.78	0.68	1.48	1.71
S4	Length (mm)	30.35	28.93	11.7	6.44	3.79	12.72	17.16	20.39	27.09	7.79	3.18	19.37
	Slope	0.04	−24.42	−1.35	−3.32	0.23	−1.13	−0.1	1.12	0.94	1.58	0.86	3.22
S5	Length (mm)	21.78	21.54	6.21	9.04	2.2	15.49	20.42	8.99	22.1	5.18	0.71	10.64
	Slope	0.98	1.29	−1.14	−4.08	−40.54	−2.31	0.4	1.72	0.92	0.54	0.31	1.19
S6	Length (mm)	34.82	34.95	17.13	14.03	10.06	12.38	44.61	29.54	20.68	6.44	0.49	32.06
	Slope	0.26	3.22	0.02	−25.76	−8.05	−2.31	0.28	1.54	0.91	1.48	8.25	2.34
S7	Length (mm)	16.77	24.49	14.08	10.98	4.28	4.38	6.93	24.36	23.04	6.24	1.72	15.75
	Slope	0.48	2.11	−3.57	1.55	0.36	−1.77	−0.78	1.24	1	0.85	0.98	1.98

Table 6. Statistical values of standard deviation for each station.

		Sep.–Oct.	Oct.–Nov.	Nov.–Dec.	Dec.–Jan.	Jan.–Feb.	Feb.–Mar.	Mar.–Apr.	Apr.–May.	May–Jun.	Jun.–Jul.	Jul.–Aug.	Aug.–Sep.
S1	Length (mm)	35.36	18.79	28.57	28.56	12.43	10.24	20.15	3.35	21.22	6.51	3.78	14.13
	Slope	0.04	−2.01	−0.54	−2.72	2.27	1.04	0.29	0.51	1.15	0.24	0.23	1.27
S2	Length (mm)	38.28	5.47	2.77	18.79	32.63	17.99	18.58	25.61	29.39	21.08	7.62	12.51
	Slope	0.59	−0.12	1.78	−59.02	−0.50	0.71	−5.94	2.60	0.52	0.87	1.41	1.51
S3	Length (mm)	24.79	20.11	25.16	35.18	23.24	3.72	7.91	15.48	45.38	10.62	6.37	13.31
	Slope	0.49	1.93	0.98	0.72	0.74	0.21	−1.28	−0.14	0.94	0.63	2.02	1.08
S4	Length (mm)	41.41	31.88	4.35	7.92	10.69	7.75	14.01	18.20	24.14	10.44	10.83	8.64
	Slope	0.02	−0.43	−1.33	2.23	−0.20	0.25	−3.00	7.56	0.72	2.62	0.84	9.53
S5	Length (mm)	20.24	6.71	6.44	5.04	8.19	6.23	5.58	4.70	30.57	5.39	1.90	8.03
	Slope	0.71	−0.79	0.93	−11.14	0.01	0.83	2.37	−0.01	0.72	0.87	−0.28	1.05
S6	Length (mm)	53.28	23.71	6.38	8.01	7.45	1.82	6.86	31.43	24.63	7.46	2.34	27.72
	Slope	0.03	−1.64	0.24	−1.08	0.18	0.24	−1.56	1.77	0.48	0.79	−1.38	2.24
S7	Length (mm)	24.07	13.97	5.22	8.05	5.29	2.24	14.22	25.40	14.74	8.41	2.04	14.20
	Slope	0.19	−1.15	16.40	−4.38	−1.09	0.64	2.28	1.14	1.34	1.20	0.93	1.07

As regards the standard deviation (Table 6), in the Souk El Had station a maximum trend length of 35.36 mm and a maximum trend slope of −2.72 were detected in September–October and December–January, respectively. Results for the Bordj Bou Naama station evidenced that the maximum trend length is 38.28 mm in September–October, while the maximum trend slope is −59.02 in December–January. As regards the Ain Lellou Mf station, the maximum trend length was identified in May–June. (45.38 mm), while the maximum trend slope is in July–August (2.02). A maximum trend length of 41.41 mm and a maximum trend slope of 9.53 were detected in the Ouled Ben A.E.K. station for the transitions September–October and August–September, respectively. In the Oued Sly station, the maximum trend length and slope were identified in May–June (30.57 mm) and December–January (−11.14), respectively. In the Saadia station, in September–October, a maximum trend length of 53.28 mm and a maximum trend slope of 2.24 in August–

September were evaluated. Finally, in the Sidi Yakoub Bge station, a maximum trend length of 25.40 mm in April–May and a maximum trend slope of 16.40 in November–December were detected.

3.2. Comparison between the IPTA Method Results and Other Tests Results

The MK and Theil-Sen incline estimator tests were applied at monthly and annual time scales to each station. The MK test statistics ($\alpha = 0.05$) show increasing ($Z > 0$) and decreasing ($Z < 0$) trends. Table 7 presents the results of trend analysis for monthly and annual sums of precipitation based on the following methods: Mann–Kendall test (MK) and Sen's slope estimator.

Table 7. Results of MK and Sen's slope (SS) methods on monthly and annual scales at the study area.

		Sep.	Oct.	Nov.	Dec.	Jan.	Feb.	Mar.	Apr.	May	Jun.	Jul.	Aug.	Year
S1	MK	1.263	0.351	1.506	−2.125 *	−1.104	−0.427	−1.623	−2.484 *	−0.895	−0.402	0.050	0.928	−1.606
	SS	0.156	0.054	0.467	−0.907	−0.495	−0.211	−0.557	−0.650	−0.041	0.000	0.000	0.000	−2.565
S2	MK	2.158 *	0.552	1.280	−0.309	1.205	0.443	−0.017	−1.882 +	−0.770	−0.694	0.443	−0.059	0.368
	SS	0.197	0.098	0.466	−0.140	0.544	0.188	−0.025	−0.683	0.000	0.000	0.000	0.000	0.629
S3	MK	0.995	−0.017	2.091 *	0.393	0.284	0.167	−1.054	−1.246	−0.795	−1.113	−0.945	−0.243	−0.167
	SS	0.105	−0.005	0.827	0.090	0.122	0.074	−0.347	−0.358	0.000	0.000	0.000	0.000	−0.245
S4	MK	1.305	−0.309	0.363	−1.288	0.000	0.301	−1.188	−1.121	−0.418	−0.485	−1.113	−1.690 +	−0.452
	SS	0.145	−0.047	0.384	−0.360	0.000	0.095	−0.420	−0.283	−0.059	0.000	0.000	0.000	−0.531
S5	MK	0.243	0.460	0.602	−1.179	0.151	0.560	−0.803	−0.711	−0.903	−1.062	−0.159	−0.326	−0.368
	SS	0.012	0.064	0.158	−0.387	0.039	0.160	−0.245	−0.150	−0.075	0.000	0.000	0.000	−0.353
S6	MK	1.322	0.402	1.690 +	−0.728	−0.619	−0.652	−0.770	1.113	1.489	2.233 *	2.183 *	2.359 *	−0.435
	SS	0.140	0.090	0.681	−0.430	−0.284	−0.265	−0.340	0.128	0.051	0.026	0.000	0.000	−1.064
S7	MK	1.263	0.703	1.874 +	−1.330	−0.728	0.142	−0.075	−1.096	−0.703	−1.380	−4.065 ***	−2.166 *	−0.084
	SS	0.122	0.109	0.504	−0.380	−0.141	0.037	−0.018	−0.262	−0.135	−0.005	0.005	−0.029	−0.124

+: significance level 0.1; *: significance level 0.05; significance level 0.01; ***: significance level 0.001.

Figure 5 shows, as an example, the sums of monthly (September, December, and March) and annual precipitation in the Oued Sly station, where no statistically significant trends were detected. A figure with all the months (Figure A1) can be found in Appendix A. This variability is well shown by modeling the precipitation by a moving average (MA) of a period of 3 years. This figure shows that trends of monthly sum of precipitation are well reflected by IPTA method (Figure 3 and Table 3), with similar trend signs. Considering the monthly sums of precipitation, a high variability is visible; conversely, in the case of annual sums, seasonality of precipitation is noticeable. The statistical significance trend of monthly precipitation was detected only with the MK test, while the trend magnitude was evaluated with the Sen's slope method. Only in the S5 station, the MK method did not detect any statistically significantly trends of monthly precipitation. In two stations, S6 and S7, located in the middle of the Wadi basin, a statistically significant trend was detected in 4 and 3 months, respectively. In the remaining stations, statistically significant trends were identified mainly in 2 months, in November and August, when the statistically significant trends were detected three times. Moreover, increasing trends were visible more often than decreasing trends. In fact, from the comparison of the results of Table 7, an increasing trend of monthly precipitations in almost all stations in September and November is evident, while in December, March, April, and May, a decreasing trend of precipitation is shown.

As regards the Sen's slope estimator, this method identified a further lack of trends than other methods. In the case of the annual sum of precipitation, in all stations decreasing and statistical insignificantly trends of precipitation were detected. The only exception is station S2, where an increasing non-significant trend was identified. A similar comparison of the IPTA method with commonly used MK test showed Alifujiang et al. [53], where they did not detect significant differences between both methods. Moreover, they concluded that the IPTA method allows more detailed interpretations about trend analysis, like benefits for identifying hidden variation trends of precipitation in comparison to commonly used

methods. Also, Saplıoğlu and Kilit [54] detected a strong correlation between results from the IPTA method in the MK test and examined discharged data in the Western Mediterranean Basin.
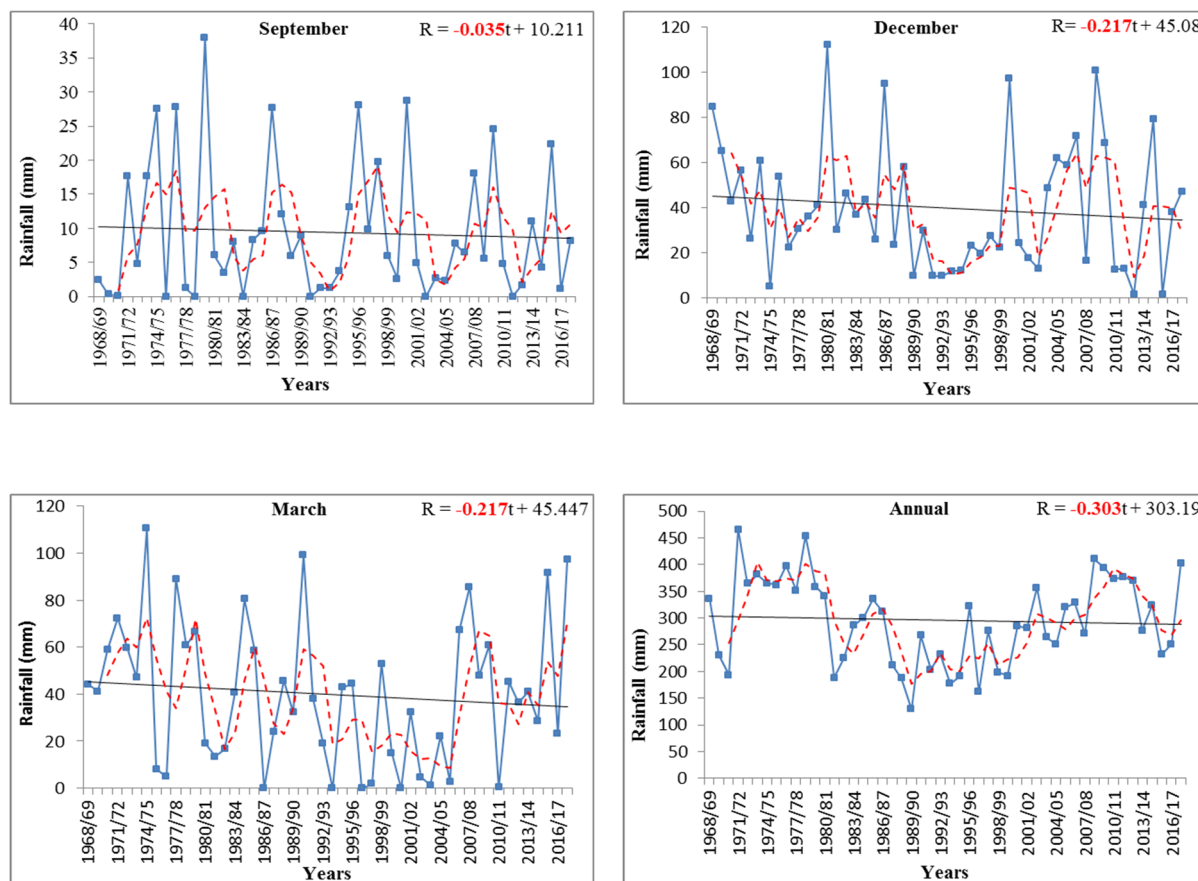

Figure 5. Sums of monthly and annual precipitation in the Oued Sly station.

From the comparison of the results obtained with the IPTA method (Tables 3 and 4) with the ones obtained with commonly used methods for trend detection (Table 7), a good agreement emerges. In fact, as Rathnayake [55] showed, results of the trend analyses for time series data with different resolutions performed with the Innovative Trend Analysis technique can give similar results to the ones obtained with the classical statistical trend analysis techniques. The author concluded that the Innovative Method is easy to perform and has low computational cost in comparison to other methods. Therefore, the technique can be widely used to identify the trends. Indeed, as mentioned earlier, the IPTA method is very simple to use from a practical point of view and has no flaws when compared to commonly used statistical tests. The method can indicate transition between analyzed months that can lead to deep analysis behavior of analyzed data. However, this technique does not provide any numerical value of the trend. Based on Şan et al. [56], it can be concluded that the IPTA method is more sensitive in detecting trends in comparison to the Mann–Kendall (MK) test. The disadvantages according to IPTA are that MK does not show a trend slope and that MK shows a holistic trend. The IPTA method has some advantages in comparison to other commonly used tests. In fact, the method is less sensitive to the influence of outlier values on final results. For example, Zittis [57] studied trends of monthly precipitation and showed that the Kruskal–Wallis test is sensitive to an outlier value. Also, the assessment of trends using commonly known methods in the characteristics of precipitation is complicated by the quality of the observations and by the intrinsic noisiness of the records [58]. Moreover, null hypothesis significance tests have a

logically flawed rationale coming from ill posed and theoretically unfounded hybridization of Fisher significance tests and Neyman–Pearson hypothesis tests. They do not allow conclusions about the truth or falsehood of any hypothesis, and do not apply to exploratory non-randomized studies [30]. In addition, statistical significance does not imply physical significance because the former depends on the sample size, and almost every test assigns statistical significance to physically negligible differences for very large samples. On the other hands, Serinaldi et al. [59], based on numerical experiments, detected many flaws of ITA methods (the IPTA is a modified version of the ITA method) like: (1) " . . . ITA diagrams are equivalent to well-known two-sample quantile-quantile (q–q) plots; (2) when applied to finite-size samples, ITA diagrams do not enable the type of trend analysis that it is supposed to do; (3) the expression of ITA confidence intervals quantifying the uncertainty of ITA diagrams is mathematically incorrect; and (4) the formulation of the formal tests is also incorrect and their correct version is equivalent to a standard parametric test for the difference between two means. Overall, we show that ITA methodology is affected by sample size, distribution shape, and serial correlation as any parametric technique devised for trend analysis". Despite many advantages, the IPTA method has similar flaws like ITA methods. Due to this reason, the IPTA method should be used only as a qualitative tool to support other methods when detecting the trend of hydrometeorological data.

4. Conclusions

In this study, the Innovative Polygon Trend Analysis Method was applied to total monthly precipitation data of seven stations in the Wadi Sly Basin in a 50-year period (1969–2018). As a result of the study, IPTA graphics were created for each station. In addition, trend lengths and trend slopes of monthly total precipitation data of each station were calculated. Additionally, results from the IPTA method were compared to two non-parametric tests: Mann–Kendall and Sen's slope estimator. After these analyses, the following evaluations were made:

- Size of trend lengths and trend slopes show the variability between months. For example, for Bordj Bou Naama Station, maximum trend lengths for arithmetic mean and standard deviation are 43.25 mm and 38.28 mm, respectively, while values of 3.32 and -59.02 are obtained for the maximum trend slopes, respectively. These values show that the transition between 2 months is severe.
- Results from the IPTA method have good agreement with commonly used non-parametric tests for each month.
- The IPTA method can be used to quantitively analyze and detect trends and can support results from other commonly used methods. The results from Man–Kendall test and Sen's estimator are quite similar. The directions of the trend are the same in most cases in both methods.

Author Contributions: Conceptualization, M.A. and G.C.; methodology, M.A., G.C. and A.I.C.; software, M.A., G.C. and A.I.C.; validation, M.A., G.C., T.C. and A.W.; formal analysis, M.A. and A.W.; investigation, M.A., A.W.; resources, M.A. and A.W.; data curation, M.A.; writing—original draft preparation, M.A., G.C., T.C. and A.W.; writing—review and editing, M.A. and A.W.; visualization, A.W.; supervision, M.A. and A.W. All authors have read and agreed to the published version of the manuscript.
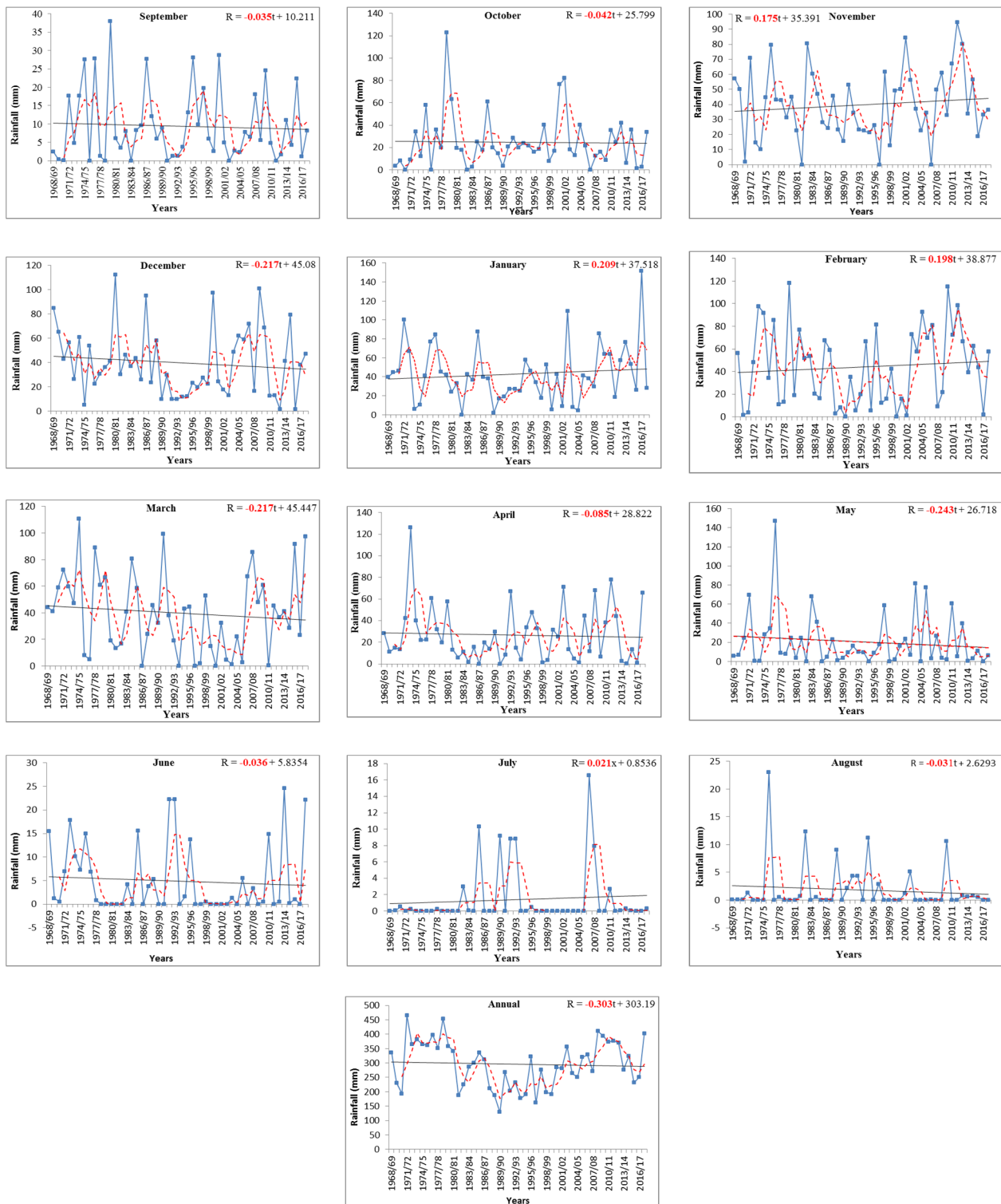
Appendix A

Figure A1. Sums of monthly and annual precipitation in the Oued Sly station.

References

1. Rana, A.; Moradkhani, H.; Qin, Y. Understanding the joint behavior of temperature and precipitation for climate change impact studies. *Theor. Appl. Climatol.* **2017**, *126*, 321–339. [CrossRef]
2. Gautam, R.; Hsu, N.C.; Lau, K.M.; Tsay, S.C.; Kafatos, M. Enhanced pre-monsoon warming over the Himalayan-Gangetic region from 1979 to 2007. *Geophys. Res. Lett.* **2009**, *36*, L07704. [CrossRef]
3. Chen, F.H.; Huang, W.; Jin, L.Y.; Chen, J.H.; Wang, J.S. Spatiotemporal precipitation variations in the arid central Asia in the context of global warming. *Sci. China Earth Sci.* **2011**, *54*, 1812–1821. [CrossRef]
4. Skowera, B.; Kopcińska, J.; Ziernicka-Wojtaszek, A.; Wojkowski, J. Niedobory i nadmiary opadów w okresie wegetacji ziemniaka późnego w województwie opolskim (1981–2010). Precipitation deficiencies and excesses during the growing season of late potato in the opolskie voivodship (1981–2010). *Acta Sci. Pol. Form. Circumiectus* **2016**, *15*, 137–149. [CrossRef]
5. Dad, J.M.; Muslim, M.; Rashid, I.; Reshi, Z.A. Time series analysis of climate variability and trends in Kashmir Himalaya. *Ecol. Indic.* **2021**, *126*, 107690. [CrossRef]
6. Juez, C.; Peña-Angulo, D.; Khorchani, M.; Regues, D.; Nadal-Romero, E. 20-years of hindsight into hydrological dynamics of a mountain forest catchment in the Central Spanish Pyrenees. *Sci. Total Environ.* **2021**, *766*, 142610. [CrossRef]
7. Amatya, D.M.; Campbell, J.; Wohlgemuth, P.; Elder, K.; Sebestyen, S.; Johnson, S.; Keppeler, E.; Adams, M.B.; Caldwell, P.; Misra, D. Hydrological processes of reference watersheds in Experimental Forests, USA. In *Forest Hydrology: Processes, Management, and Applications*; Amatya, D.M., Williams, T.M., Bren, L., de Jong, C., Eds.; CABI Publishers: Wallingford, UK, 2016; pp. 219–239.
8. Amatya, D.M.; Skaggs, R.W.; Blanton, C.D.; Gilliam, J.W. Hydrologic and water quality effects of harvesting and regeneration of a drained pine forest. In Proceedings of the International Conference Hydrology and Management of Forested Wetlands, New Bern, NC, USA, 8–12 April 2006; American Society of Agricultural and Biological Engineers: St. Joseph, MI, USA; pp. 538–551.
9. Muwamba, A.; Amatya, D.M.; Ssegane, H.; Chescheir, G.M.; Appelboom, T.; Nettles, J.E.; Tollner, E.W.; Youssef, M.A.; Walega, A.; Birgand, F. Response of Nutrients and Sediment to Hydrologic Variables in Switchgrass Intercropped Pine Forest Ecosystems on Poorly Drained Soil. *Water Air Soil Pollut.* **2020**, *231*, 458. [CrossRef]
10. Achite, M.; Caloiero, T.; Wałęga, A.; Krakauer, N.; Hartani, T. Analysis of the Spatiotemporal Annual Rainfall Variability in the Wadi Cheliff Basin (Algeria) over the Period 1970 to 2018. *Water* **2021**, *13*, 1477. [CrossRef]
11. Almendra-Martín, L.; Martínez-Fernández, J.; González-Zamora, Á.; Benito-Verdugo, P.; Herrero-Jiménez, C.M. Agricultural Drought Trends on the Iberian Peninsula: An Analysis Using Modeled and Reanalysis Soil Moisture Products. *Atmosphere* **2021**, *12*, 236. [CrossRef]
12. Fellag, M.; Achite, M.; Wałęga, A. Spatial-temporal characterization of meteorological drought using the Standardized precipitation index. Case study in Algeria. *Acta Sci. Pol. Form. Circumiectus* **2021**, *20*, 19–31.
13. Zhou, J.; Wang, Y.; Su, B.; Wang, A.; Tao, H.; Zhai, J.; Kundzewicz, Z.; Jiang, T. Choice of potential evapotranspiration formulas influences drought assessment: A case study in China. *Atmos. Res.* **2020**, *242*, 104979. [CrossRef]
14. Młyński, D.; Cebulska, M.; Wałęga, A. Trends, Variability, and Seasonality of Maximum Annual Daily Precipitation in the Upper Vistula Basin, Poland. *Atmosphere* **2018**, *9*, 313. [CrossRef]
15. Parry, S.; Prudhomme, C.; Hannaford, J.; Lloyd-Hughes, B. Examining the spatio-temporal evolution and characteristics of large-scale European droughts. In Proceedings of the BHS Third International Symposium, Newcastle, UK, 19–23 July 2010; British Hydrological Society: London, UK, 2010; pp. 135–142.
16. Kingston, D.G.; Stagge, J.H.; Tallaksen, L.M.; Hannah, D.M. European-Scale Drought: Understanding Connections between Atmospheric Circulation and Meteorological Drought Indices. *J. Clim.* **2015**, *28*, 505–516. [CrossRef]
17. Littmann, T. An empirical classification of weather types in the Mediterranean Basin and their interrelation with rainfall. *Theor. Appl. Clim.* **2000**, *66*, 161–171. [CrossRef]
18. Hu, Y.; Wang, S. Associations between winter atmospheric teleconnections in drought and haze pollution over Southwest China. *Sci. Total Environ.* **2021**, *766*, 142599. [CrossRef]
19. Zhang, Y.; Wu, R. Asian meteorological droughts on three time scales and different roles of sea surface temperature and soil moisture. *Int. J. Climatol.* **2021**, *41*, 6047–6064. [CrossRef]
20. Caloiero, T.; Caloiero, P.; Frustaci, F. Long-term precipitation trend analysis in Europe and in the Mediterranean basin. *Water Environ. J.* **2018**, *32*, 433–445. [CrossRef]
21. Buttafuoco, G.; Caloiero, T.; Coscarelli, R. Analyses of drought events in Calabria (Southern Italy) using standardized precipitation index. *Water Resour. Manag.* **2015**, *29*, 557–573. [CrossRef]
22. Elouissi, A.; Sen, Z.; Habi, M. Algerian rainfall innovative trend analysis and its implications to Macta watershed. *Arab. J. Geosci.* **2016**, *9*, 303. [CrossRef]
23. Bağçaci, S.Ç.; Yucel, I.; Duzenli, E.; Yilmaz, M.T. Intercomparison of the expected change in the temperature and the precipitation retrieved from CMIP6 and CMIP5 climate projections: A Mediterranean hot spot case, Turkey. *Atmos. Res.* **2021**, *256*, 105576. [CrossRef]
24. El-Geziry, T.M. Monthly and annual variations in the rainfall pattern along the Southern Levantine Coastline. *Res. Mar. Sci.* **2021**, *6*, 915–925.
25. Ali, R.O.; Abubaker, S.R. Trend analysis using mann-kendall, sen's slope estimator test and innovative trend analysis method in Yangtze river basin, China: Review. *Int. J. Eng. Technol.* **2019**, *8*, 110–119.

26. Onyutha, C. Identification of sub-trends from hydro-meteorological series. *Stoch. Environ. Res. Risk Assess.* **2015**, *30*, 189–205. [CrossRef]
27. Blain, G.C. The Mann-Kendall test the need to consider the interaction between serial correlation and trend. *Acta Sci. Agron.* **2013**, *36*, 393–402.
28. Yue, S.; Wang, C.Y. The Mann-Kendall test modified by effective sample size to detect trend in serially correlated hydrological series. *Water Resour. Manag.* **2004**, *18*, 201–218. [CrossRef]
29. Wang, F.; Shao, W.; Yu, H.; Kan, G.; He, X.; Zhang, D.; Ren, M.; Wang, G. Re-evaluation of the Power of the Mann-Kendall Test for Detecting Monotonic Trends in Hydrometeorological Time Series. *Front. Earth Sci.* **2020**, *8*, 14. [CrossRef]
30. Serinaldi, F.; Kilsby, C.G.; Lombardo, F. Untenable nonstationarity: An assessment of the fitness for purpose of trend tests in hydrology. *Adv. Water Resour.* **2018**, *111*, 132–155. [CrossRef]
31. Şen, Z. Innovative Trend Analysis Methodology. *J. Hydrol. Eng.* **2012**, *17*, 1042–1046. [CrossRef]
32. Caloiero, T.; Coscarelli, R.; Ferrari, E. Application of the Innovative Trend Analysis Method for the Trend Analysis of Rainfall Anomalies in Southern Italy. *Water Resour. Manag.* **2018**, *32*, 4971–4983. [CrossRef]
33. Caloiero, T. Evaluation of rainfall trends in the South Island of New Zealand through the innovative trend analysis (ITA). *Theor. Appl. Climatol.* **2020**, *139*, 493–504. [CrossRef]
34. Gedefaw, M.; Yan, D.; Wang, H.; Qin, T.; Girma, A.; Abiyu, A.; Batsuren, D. Innovative Trend Analysis of Annual and Seasonal Rainfall Variability in Amhara Regional State, Ethiopia. *Atmosphere* **2018**, *9*, 326. [CrossRef]
35. Haktanir, T.; Citakoglu, H. Trend, independence, stationarity, and homogeneity tests on maximum rainfall series of standard durations recorded in Turkey. *J. Hydrol. Eng.* **2014**, *19*, 501–509. [CrossRef]
36. Malik, A.; Kumar, A.; Guhathakurta, P.; Kisi, O. Spatial-temporal trend analysis of seasonal and annual rainfall (1966–2015) using innovative trend analysis method with significance test. *Arab. J. Geosci.* **2019**, *12*, 328. [CrossRef]
37. Almazroui, M.; Şen, Z. Trend Analyses Methodologies in Hydro-meteorological Records. *Earth Syst. Environ.* **2020**, *4*, 713–738. [CrossRef]
38. Ceribasi, G.; Ceyhunlu, A.I.; Ahmed, N. Innovative trend pivot analysis method (ITPAM): A case study for precipitation data of Susurluk Basin in Turkey. *Acta Geophys.* **2021**, *69*, 1465–1480. [CrossRef]
39. Ceribasi, G.; Ceyhunlu, A.I. Analysis of total monthly precipitation of Susurluk Basin in Turkey using innovative polygon trend analysis method. *J. Water Clim. Chang.* **2021**, *12*, 1532–1543. [CrossRef]
40. Sen, Z.; Sisman, E.; Dabanli, I. Innovative Polygon Trend Analysis (IPTA) and applications. *J. Hydrol.* **2019**, *575*, 202–210. [CrossRef]
41. Mann, H.B. Nonparametric Tests against Trend. *Econometrica* **1945**, *13*, 245–259. [CrossRef]
42. Kendall, M.G. *Rank Correlation Methods*; Griffin: Oxford, UK, 1975.
43. Sen, P.K. Estimates of the Regression Coefficient Based on Kendall's Tau. *J. Am. Stat. Assoc.* **1968**, *63*, 1379–1389. [CrossRef]
44. Achite, M.; Caloiero, T. Analysis of temporal and spatial rainfall variability over the Wadi Sly basin, Algeria. *Arab. J. Geosci.* **2021**, *14*, 1867. [CrossRef]
45. Dettinger, M.D.; Cayan, D.R. Drought and the California delta—A matter of extremes. *San Franc. Est. Watershed Sci.* **2014**, *12*, 2–6. [CrossRef]
46. Polade, S.D.; Gershunov, A.; Cayan, D.R.; Dettinger, M.D.; Pierce, D.W. Precipitation in a warming world: Assessing projected hydro-climate changes in California and other Mediterranean climate regions. *Sci. Rep.* **2017**, *7*, 10783. [CrossRef]
47. Favre, A.; Gershunov, A. North Pacific cyclonic and anticyclonic transients in a global warming context: Possible consequences for Western North American daily precipitation and temperature extremes. *Clim. Dyn.* **2009**, *32*, 969–987. [CrossRef]
48. Meddi, M.M.; Assani, A.A.; Meddi, H. Temporal Variability of Annual Rainfall in the Macta and Tafna Catchments, Northwestern Algeria. *Water Resour. Manag.* **2010**, *24*, 3817–3833. [CrossRef]
49. Tramblay, Y.; El Adlouni, S.; Servat, E. Trends and variability in extreme precipitation indices over Maghreb countries. *Nat. Hazards Earth Syst. Sci.* **2013**, *13*, 3235–3248. [CrossRef]
50. Driouech, F.; Rached, S.B.; Hairech, T.E. Climate Variability and Change in North African Countries. In *Climate Change and Food Security in West Asia and North Africa*; Springer: Dordrecht, The Netherlands, 2013; pp. 161–172.
51. Lionello, P.; Bhend, J.; Buzzi, A.; Della-Marta, P.M.; Krichak, S.O.; Jansa, A.; Maheras, P.; Sanna, A.; Trigo, I.F.; Trigo, R. Cyclones in the Mediterranean Region: Climatology and Effects on the Environment. In *Mediterranean Climate Variability*; Elsevier: Amsterdam, The Netherlands, 2006; pp. 325–372.
52. Nouaceur, Z.; Murarescu, O.; Mură Rescu, O. Rainfall Variability and Trend Analysis of Annual Rainfall in North Africa. *Int. J. Atmos. Sci.* **2016**, *2016*, 1–12. [CrossRef]
53. Alifujiang, Y.; Abuduwaili, J.; Maihemuti, B.; Emin, B.; Groll, M. Innovative Trend Analysis of Precipitation in the Lake Issyk-Kul Basin, Kyrgyzstan. *Atmosphere* **2020**, *11*, 332. [CrossRef]
54. Saplıoğlu, K.; Kilit, M.; Yavuz, B.K. Trend analysis of streams in the Western Mediterranean Basin of Turkey. *Fresenius Environ. Bull.* **2014**, *23*, 313–324.
55. Rathnayake, U. Comparison of Statistical Methods to Graphical Methods in Rainfall Trend Analysis: Case Studies from Tropical Catchments. *Adv. Meteorol.* **2019**, *2019*, 8603586. [CrossRef]
56. Şan, M.; Akçay, F.; Linh, N.T.T.; Kankal, M.; Pham, Q.B. Innovative and polygonal trend analyses applications for rainfall data in Vietnam. *Theor. Appl. Climatol.* **2021**, *144*, 809–822. [CrossRef]

57.   Zittis, G. Observed rainfall trends and precipitation uncertainty in the vicinity of the Mediterranean, Middle East and North Africa. *Theor. Appl. Climatol.* **2018**, *134*, 1207–1230. [CrossRef]

58.   Biasutti, M. Rainfall trends in the African Sahel: Characteristics, processes, and causes. *Wiley Interdiscip. Rev. Clim. Chang.* **2019**, *10*, e591. [CrossRef] [PubMed]

59.   Serinaldi, F.; Chebana, F.; Kilsby, C.G. Dissecting innovative trend analysis. *Stoch. Environ. Res. Risk Assess.* **2020**, *34*, 733–754. [CrossRef]